Article

Hinged and Wide: A New PˆP Ligand for Emissive [Cu(PˆP)(NˆN)][PF$_6$] Complexes

Sarah Keller [1,2] **, Matthias Bantle** [1] **, Alessandro Prescimone** [1] **, Edwin C. Constable** [1] **and Catherine E. Housecroft** [1,*]

[1] Department of Chemistry, University of Basel, BPR 1096, Mattenstrasse 24a, CH-4058 Basel, Switzerland; sarah.keller@chimieparistech.psl.eu (S.K.); mattu.bantle@gmail.com (M.B.); alessandro.prescimone@unibas.ch (A.P.); edwin.constable@unibas.ch (E.C.C.)

[2] Chimie ParisTech, PSL University CNRS, Institute of Chemistry for Life and Health Sciences, Laboratory for Inorganic Chemical Biology, 11 rue Pierre et Marie Curie, F-75005 Paris, France

[*] Correspondence: catherine.housecroft@unibas.ch; Tel.: +41-61-207-1008

Abstract: Heteroleptic [Cu(BIPHEP)(NˆN)][PF$_6$] complexes (BIPHEP = 1,1′-biphenyl-2,2′-diylbis(diphenylphosphane)), in which NˆN is 2,2′-bipyridine (bpy), 6-methyl-2,2′-bipyridine (6-Mebpy), 6-ethyl-2,2′-bipyridine (6-Etbpy), or 5,5′-dimethyl-2,2′-bipyridine (5,5′-Me$_2$bpy), have been synthesized and characterized using multinuclear NMR spectroscopies and electrospray ionization mass spectrometry. The single crystal structures of [Cu(BIPHEP)(bpy)][PF$_6$]·CH$_2$Cl$_2$, [Cu(BIPHEP)(5,5′-Me$_2$bpy)][PF$_6$]·CH$_2$Cl$_2$, [Cu(BIPHEP)(6-Mebpy)][PF$_6$]·Et$_2$O·0.5H$_2$O and [Cu(BIPHEP)(6-Etbpy)][PF$_6$] confirm distorted tetrahedral {Cu(PˆP)(NˆN)} coordination environments. Each compound shows a quasi-reversible Cu$^+$/Cu^{2+} process. In deaerated solution, the compounds are weak emitters. Powdered samples are yellow emitters (λ_{em}^{max} in the range 558–583 nm) and [Cu(BIPHEP)(5,5′-Me$_2$bpy)][PF$_6$] exhibits the highest photoluminescence quantum yield (PLQY = 14%). On cooling to 77 K (frozen 2-methyloxolane), the emission maxima are red-shifted and the excited state lifetimes increase from $\tau_{1/2}$ < 8 µs, to $\tau_{1/2}$ values of up to 53 µs, consistent with the compounds with NˆN = 6-Mebpy, 6-Etbpy and 5,5′-Me$_2$bpy exhibiting thermally activated delayed fluorescence (TADF).

Keywords: copper(I); bis(phosphane); 2,2′-bipyridine; X-ray structure; photophysics; TADF

1. Introduction

Organic light-emitting diodes (OLEDs) and light-emitting electrochemical cells (LECs) contribute to modern solid-state lighting technologies, and significant advances in the performances of these devices have been made in recent years [1–6]. The discovery of the photophysical phenomenon of thermally activated delayed fluorescence (TADF), which allows both singlet and triplet excitons to be harvested for light emission, has injected huge excitement into the field [7–9]. In the TADF process, after excitation of a compound into the lowest-lying singlet excited state, fast intersystem crossing to the excited triplet state, at a slightly lower energy (<0.38 eV [9]), takes place. As the triplet state is long lived, and emission as phosphorescence is rather slow, the thermal energy at room temperature allows repopulation of the singlet excited state from which fluorescence occurs. The emission at room temperature is, therefore, a combination of phosphorescence from the triplet excited state and fluorescence from the singlet excited state, allowing, in theory, a 100% internal quantum efficiency. Although organic compounds have been widely used for TADF applications [10,11] metal complexes are particularly effective and can be easily tuned through ligand modification to possess desired excited state energies [9]. The development of LECs which contain ionic copper(I) complexes in the

emissive layer is especially appealing, since it capitalizes on the use of an Earth-abundant metal and [Cu(PˆP)(NˆN)]⁺ complexes (NˆN = diimine, PˆP = bisphosphane) which exhibit TADF [9]. Application of these copper(I) coordination compounds follows early results from McMillin and co-workers, who were the first to report that copper(I) complexes comprising PPh₃ or PˆP ligands and 2,2′-bipyridine (bpy) or 1,10-phenanthroline (phen) exhibited low-lying metal-to-ligand charge transfer (MLCT) excited states [12,13].

To date, the PˆP ligands most thoroughly explored for incorporation into emissive [Cu(PˆP)(NˆN)]⁺ complexes have been 4,5-bis(diphenylphosphanyl)-9,9-dimethyl-9*H*-xanthene (xantphos, IUPAC PIN (9,9-dimethyl-9*H*-xanthene-4,5-diyl)bis(diphenylphosphane)) and bis(2-(diphenylphosphanyl)phenyl)ether (POP, IUPAC PIN oxydi(2,1-phenylene)]bis(diphenylphosphane)) (Scheme 1). Both are classed as wide bite–angle bisphosphanes [14], and the P–Cu–P bite angles in the solid-state structures of [Cu(POP)(bpy)][PF₆]·CHCl₃, [Cu(POP)(bpy)][PF₆]·Et₂O and [Cu(xantphos)(bpy)][PF₆] are 115.00(3)° [15], 111.97(3)° [16] and 113.816(14) [17], respectively. A wide variety of bpy-based ligands have been combined with POP and xantphos in systematic investigations of [Cu(PˆP)(NˆN)]⁺ emitters [3,17–23] and references cited therein]. In contrast, variations of the PˆP ligand (other than POP and xantphos) have received less attention. Replacing the PPh₂ units in xantphos with PMes₂ units (Mes = mesityl) leads to a P–Cu–P angle in [Cu(xantphosMes₂)(bpy)][PF₆] (xantphosMes₂ = 9,9-dimethyl-9*H*-xanthene-4,5-diyl)bis[di(2,4,6-trimethylphenyl)phosphane]) of 115.96(2)° [24]. We have observed that introducing P^{t}Bu₂ in place of PPh₂ groups in the xantphos derivative 9,9-dimethyl-9*H*-xanthene-4,5-diyl)bis[di(*tert*-butyl)phosphane] is detrimental, and gives rise to very weakly emitting [Cu(PˆP)(NˆN)][PF₆] compounds, likely due to the vibrational quenching effects of the *tert*-butyl substituents [25]. Retaining aromatic substituents is therefore critical for efficient energy to light conversion. Two sterically demanding ligands that fulfil this requirement are 1,1′-biphenyl-2,2′-diylbis(diphenylphosphane) (BIPHEP) and 1,1′-binaphthalene-2,2′-diylbis(diphenylphosphane) (BINAP) (Scheme 1). A search of the Cambridge Structural Database (v. 5.40 with February 2019 updates [26]) for {Cu(BINAP)(NˆN)}-containing compounds, in which NˆN is constrained to a chelating ligand, reveals only six entries [27–30] and for these, the range of P–Cu–P bond angles is 99.25–105.13°. Both BINAP and BIPHEP are expected to exhibit atropisomerism, but, at room temperature, interconversion of (*R*)- and (*S*)-BINAP is slow, whereas the atropisomers (*R*)- and (*S*)-BIPHEP (Scheme 1) interconvert rapidly in solution [31]. Coordination of BIPHEP to a metal centre can lead to chiral metal coordination compounds. The preparation and photophysical properties of [Cu(BINAP)(NˆN)]⁺ complexes have been reported [28], but, even though BIPHEP is commercially available, no [Cu(BIPHEP)(NˆN)]⁺ complexes appear to have been described. We were, therefore, inspired to investigate the structural and solution properties of such complexes. In this work, we describe the preparation and characterization of [Cu(BIPHEP)(bpy)][PF₆], along with three derivatives, in which the bpy metal-binding domain bears alkyl substituents in the 5- or 6-positions.
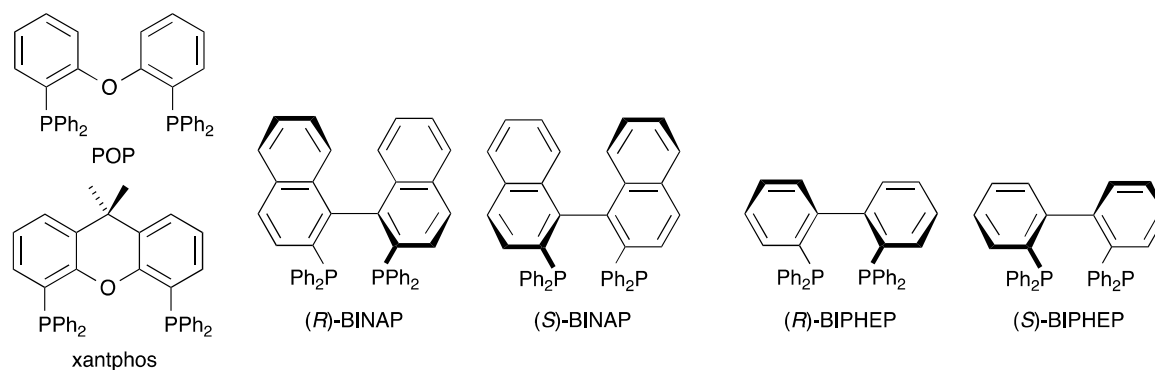

Scheme 1. Structures of the bis(phosphane) ligands POP, xantphos, BINAP and BIPHEP.

2. Results and Discussion

2.1. Synthesis and Characterization of [Cu(BIPHEP)(N^N][PF_6] Complexes

The [Cu(BIPHEP)(N^N)][PF$_6$] complexes, in which N^N is bpy, 6-Mebpy, 6-Etbpy or 5,5′-Me$_2$bpy, were prepared by adding CH$_2$Cl$_2$ solutions containing both BIPHEP and the respective 2,2′-bipyridine ligand to CH$_2$Cl$_2$ solutions of [Cu(MeCN)$_4$][PF$_6$].   This led to an immediate colour change from colourless to yellow, indicating the formation of the heteroleptic complexes without ligand redistribution; formation of a homoleptic [Cu(N^N)$_2$][PF$_6$] complex would have been accompanied by the development of a distinctive red colour.   Attempts to prepare the analogous complex [Cu(BIPHEP)(6,6′-Me$_2$bpy)][PF$_6$] resulted in a mixture of homoleptic complexes as well as the desired heteroleptic compound, and since equilibration between hetero- and homoleptic complexes persisted in the solution, this reaction was not investigated further. The compounds [Cu(BIPHEP)(bpy)][PF$_6$], [Cu(BIPHEP)(6-Mebpy)][PF$_6$], [Cu(BIPHEP)(6-Etbpy)][PF$_6$] and [Cu(BIPHEP)(5,5′-Me$_2$bpy)][PF$_6$] were characterized by elemental analysis, mass spectrometry, and multinuclear NMR spectroscopies.

In the ESI-MS spectrum of each compound, the base peak was assigned to the [M–PF$_6$]$^+$ ion (Figures S1–S4, see Supporting Information). The room temperature ^{1}H and ^{13}C{^{1}H} NMR spectra were recorded in acetone-d_6 solution and signals were assigned (see Materials and Methods section) using 2D-methods.   Aromatic ring and atom labelling are shown in Scheme 2. COSY, HMQC and HMBC spectra are displayed in Figures S5–S16 (see Supporting Information). Figure 1 shows that the signals arising from the coordinated bpy, 6-Mebpy, 6-Etbpy and 5,5′-Me$_2$bpy ligands are well resolved and sharp. The non-equivalent pyridine rings in [Cu(BIPHEP)(6-Mebpy)][PF$_6$] and [Cu(BIPHEP)(6-Etbpy)][PF$_6$] (Figure 1b,c) were readily distinguished, starting with the characteristic signal for proton H^{A6} in the COSY spectrum and using the NOESY signal between the 6-alkyl group and proton H^{B5}. In [Cu(BIPHEP)(bpy)][PF$_6$] and [Cu(BIPHEP)(5,5′-Me$_2$bpy)][PF$_6$], the ^{1}H and ^{13}C{^{1}H} NMR spectra at room temperature reveal that the rings (rings C in Scheme 1) in the biphenyl unit of BIPHEP are equivalent. Consistent with this is the observation of a single signal in the ^{31}P{^{1}H} NMR spectrum for the cation, at δ −1.2 ppm and δ −0.6 ppm, respectively, for [Cu(BIPHEP)(bpy)][PF$_6$] and [Cu(BIPHEP)(5,5′-Me$_2$bpy)][PF$_6$]. In [Cu(BIPHEP)(6-Mebpy)][PF$_6$] and [Cu(BIPHEP)(6-Etbpy)][PF$_6$], the rings of the biphenyl unit are non-equivalent, and this is illustrated by comparing Figure 1a,d with Figure 1b,c, with a splitting of the signal for the H^{C3} protons. This is consistent with the modelled structure [32] shown in Figure 2; the biphenyl rings remain non-equivalent, even with partial rotation about the trans-annular C–C bond of the biphenyl unit. At 298 K, the solution ^{31}P{^{1}H} NMR spectrum of [Cu(BIPHEP)(6-Mebpy)][PF$_6$] (Figure 3) and [Cu(BIPHEP)(6-Etbpy)][PF$_6$] (Figure S17 in the Supporting Information) exhibits two signals of similar chemical shifts, in addition to the signal for the [PF$_6$]$^-$ ion.
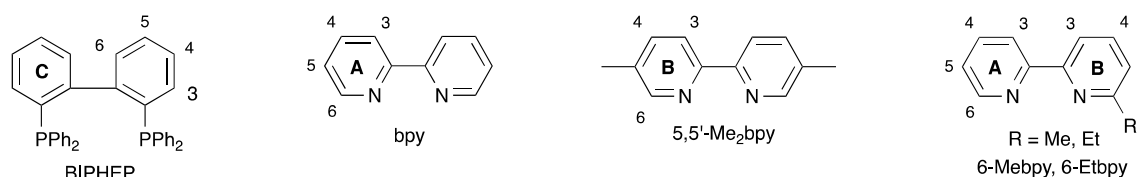

Scheme 2. The structure of the ligands and numbering scheme for NMR spectroscopic assignments. The phenyl rings in BIPHEP are labelled **D**.
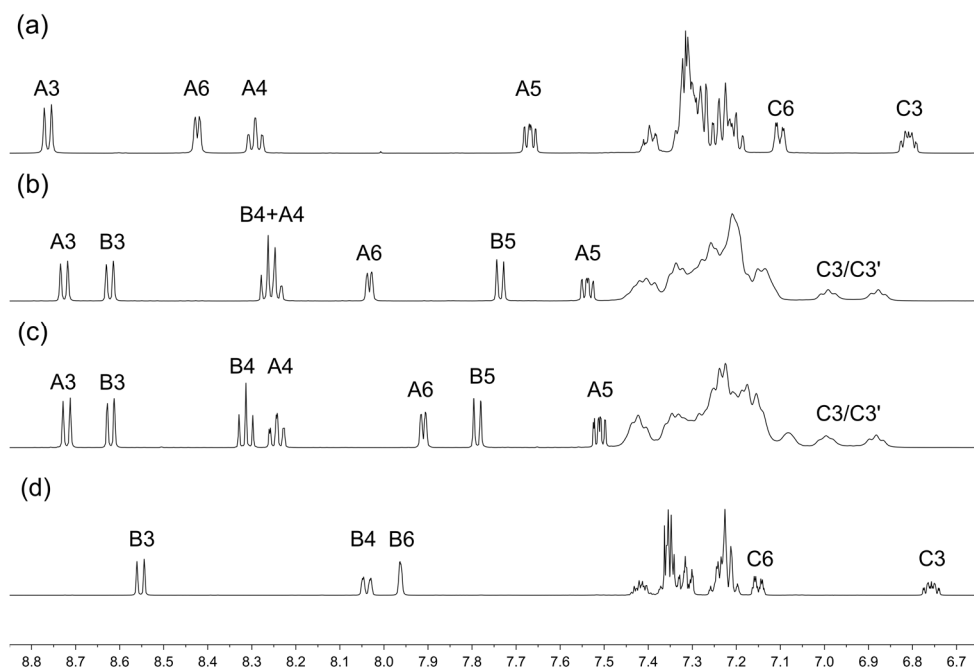
Figure 1. ^{1}H-NMR spectra (aromatic regions, 500 MHz, acetone-d_6, 298 K) of (**a**) [Cu(BIPHEP)(bpy)][PF$_6$], (**b**) [Cu(BIPHEP)(6-Mebpy)][PF$_6$], (**c**) [Cu(BIPHEP)(6-Etbpy)][PF$_6$] and (**d**) [Cu(BIPHEP)(5,5′-Me$_2$bpy)][PF$_6$].
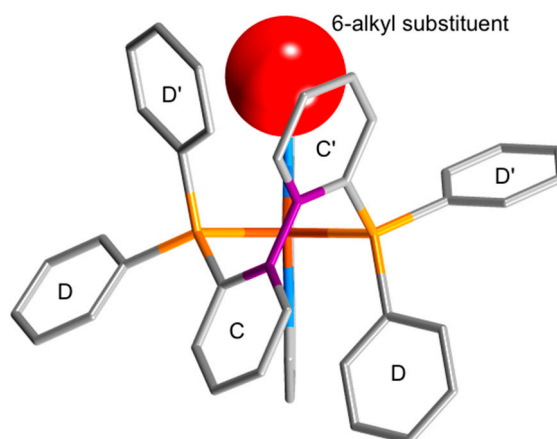

Figure 2. Modelled structure (not energy minimized) of [Cu(BIPHEP)(6-Rbpy)]$^+$, in which the alkyl group R is represented by the red sphere and the trans-annular bond in the biphenyl unit is shown in purple. Partial rotation about the latter renders the two D′ rings equivalent and the two D rings equivalent, but the pair C and C′, and the pair D and D′, remain non-equivalent.
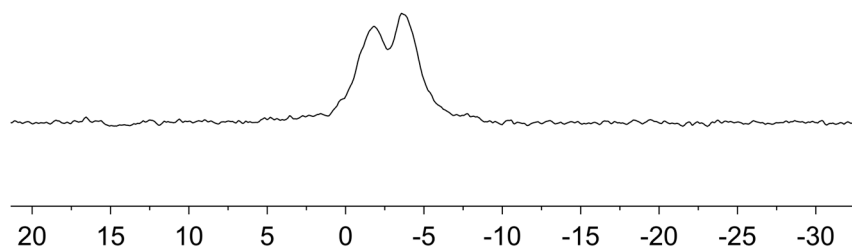
Figure 3. The signal arising from the [Cu(BIPHEP)(6-Mebpy)]$^+$ cation in the ^{31}P{^{1}H} NMR spectrum (202 MHz, acetone-d_6, 298 K) of [Cu(BIPHEP)(6-Mebpy)][PF$_6$].

We have previously discussed in detail the dynamic processes observed for complexes of the types [Cu(POP)(6-Rbpy)]$^+$ and [Cu(xantphos)(6-Rbpy)]$^+$, where 6-Rbpy is a 6-substituted 2,2′-bipyridine [19,33]. In the ^{1}H-NMR spectra in Figure 1, it is noticeable that the regions associated with the phenyl rings of the PPh$_2$ units (rings labelled D) are broader for compounds containing asymmetrical 6-Mebpy and 6-Etbpy than for those with bpy or 5,5′-Me$_2$bpy. The ^{13}C{^{1}H} NMR spectra in Figure 4 are instructive. In [Cu(BIPHEP)(bpy)][PF$_6$], all signals are well-resolved and have been assigned with the aid of HMQC and HMBC spectra. The two sets of C$^{D1/D1′}$, C$^{D2/D2′}$, C$^{D3/D3′}$ and C$^{D4/D4′}$ signals arise from pairs facing towards or away from the bpy alkyl substituent (Figure 2), and the spectra are consistent with unhindered rotation of the PPh$_2$ phenyl rings. Introducing the 6-alkyl substituent results in a broadening of all ^{13}C{^{1}H} NMR resonances arising from rings C and D (Figure 4b), consistent with increased barriers to dynamic behaviour. An inspection of the changes in line shapes of the signals for C^{D2} and C$^{D2′}$, and for C^{D3} and C^{D3} (highlighted in Figure 4 by the red hashed lines) suggests that the energy barrier to the rotation of one set of phenyls (presumably the rings closest to the alkyl substituent) is higher than that for the second set.
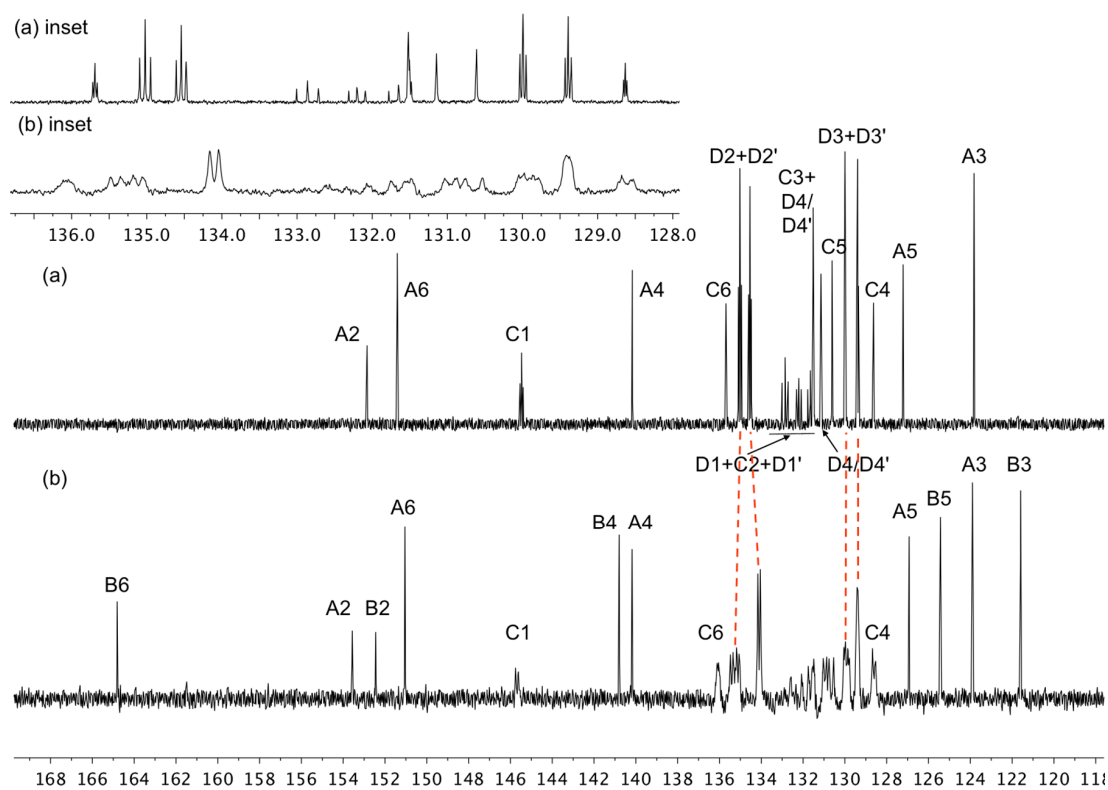

Figure 4. ^{13}C{^{1}H} NMR spectra (126 MHz, acetone-d_6, 298 K) of (**a**) [Cu(BIPHEP)(bpy)][PF$_6$] and (**b**) [Cu(BIPHEP)(6-Etbpy)][PF$_6$], with expansions of the regions δ 137–128 ppm (signals from C^{C6} to C^{C4}), shown in the insets at the top-left. Scale: δ/ppm.

2.2. Single Crystal X-ray Diffraction

X-ray quality crystals of [Cu(BIPHEP)(bpy)][PF$_6$]·CH$_2$Cl$_2$, [Cu(BIPHEP)(6-Mebpy)][PF$_6$]·Et$_2$O·0.5H$_2$O, [Cu(BIPHEP)(6-Etbpy)][PF$_6$] and [Cu(BIPHEP)(5,5′-Me$_2$bpy)][PF$_6$]·CH$_2$Cl$_2$, were obtained by diffusion of Et$_2$O into CH$_2$Cl$_2$ solutions of the respective compound. The latter two compounds crystallize in the monoclinic space groups $P2_1/c$ and $C2/c$, respectively, while [Cu(BIPHEP)(bpy)][PF$_6$]·CH$_2$Cl$_2$ and [Cu(BIPHEP)(6-Mebpy)][PF$_6$]·Et$_2$O·0.5H$_2$O crystallize in the triclinic space group $P\bar{1}$. The solid-state structures of the [Cu(BIPHEP)(N^N)]$^+$ cations are shown in Figures 5 and 6, and selected structural parameters are summarized in Table 1. The twist in the backbone of the BIPHEP ligand renders each [Cu(BIPHEP)(N^N)]$^+$ cation chiral (Figure 7), and both enantiomers are present in the unit cell.
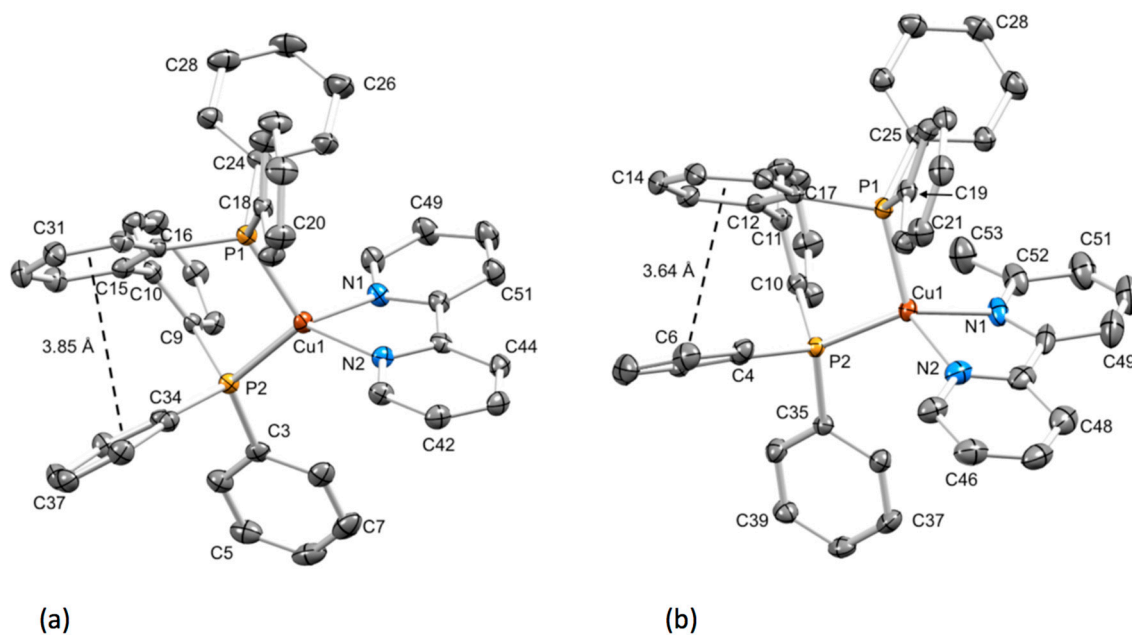
**Figure 5.** Structures of (**a**) the [Cu(BIPHEP)(bpy)]$^+$ cation in [Cu(BIPHEP)(bpy)][PF$_6$]·CH$_2$Cl$_2$ and (**b**) the [Cu(BIPHEP)(6-Mebpy)]$^+$ cation in [Cu(BIPHEP)(6-Mebpy)][PF$_6$]·Et$_2$O·0.5H$_2$O. Ellipsoids are plotted at 50% probability in (**a**) and 40% in (**b**); H atoms are omitted for clarity. Each cation exhibits π-stacking between two phenyl rings in BIPHEP backbone. In (**a**) the angle between the ring planes = 25.7°, centroid...centroid distance = 3.85 Å, and in (**b**) the angle between the ring planes = 15.1°, centroid...centroid distance = 3.64 Å.
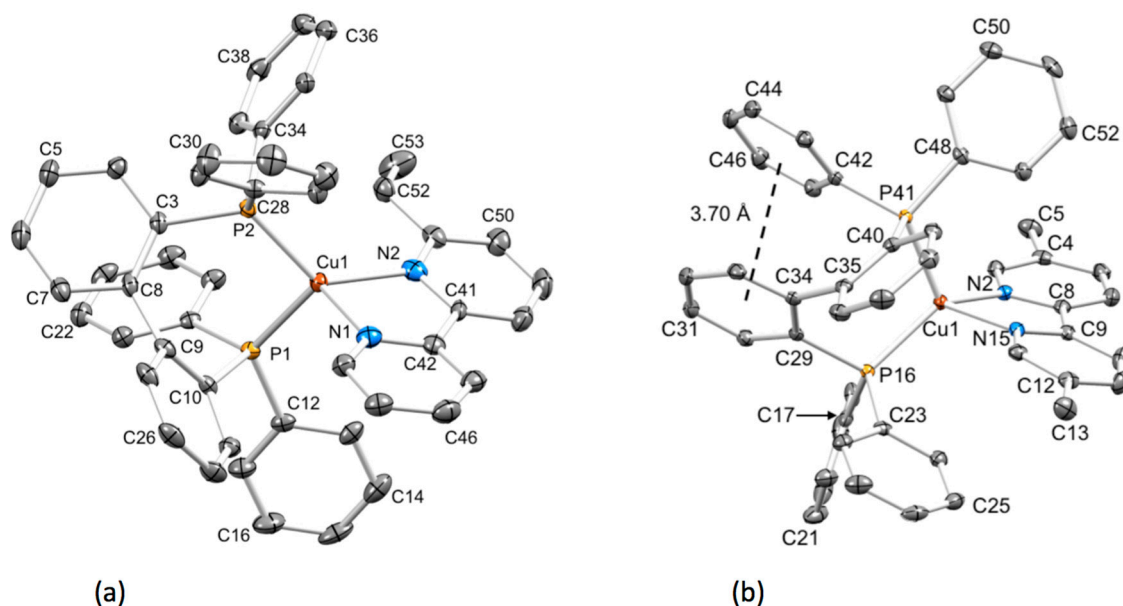
Figure 6. Structures of (**a**) the [Cu(BIPHEP)(6-Etbpy)]$^+$ cation in [Cu(BIPHEP)(6-Etbpy)][PF$_6$] and (**b**) the [Cu(BIPHEP)(5,5′-Me$_2$bpy)]$^+$ cation in [Cu(BIPHEP)(5,5′-Me$_2$bpy)][PF$_6$]·CH$_2$Cl$_2$. Ellipsoids are plotted at 40% probability in (**a**) and 50% in (**b**); H atoms are omitted for clarity. For the π-stacking interaction shown in (**b**), the angle between the ring planes is 18.0° and the centroid...centroid distance is 3.70 Å.

Table 1. Selected structural parameters for the [Cu(BIPHEP)(NˆN)][PF$_6$] compounds.

Cation in [Cu(BIPHEP)(NˆN)][PF$_6$]	Cu–P Distance/Å	Cu–N distance/Å	P–Cu–P Angle/Deg	N–Cu–N Angle/Deg	N–C–C–N Torsion Angle/Deg
[Cu(BIPHEP)(bpy)]$^+$	Cu1–P1 = 2.2415(10); Cu1–P2 = 2.2292(9)	Cu1–N1 = 2.071(3); Cu1–N2 = 2.040(3)	P2–Cu1–P1 = 104.70(4)	N2–Cu1–N1 = 80.15(11)	−11.7(5)
[Cu(BIPHEP)(6-Mebpy)]$^+$	Cu1–P1 = 2.2570(7); Cu1–P2 = 2.2549(7)	Cu1–N1 = 2.086(2); Cu1–N2 = 2.049(2)	P2–Cu1–P1 = 105.01(2)	N1–Cu1–N2 = 80.65(10)	−12.1(4)
[Cu(BIPHEP)(6-Etbpy)]$^+$	Cu1–P1 = 2.2410(11); Cu1–P2 = 2.2322(10)	Cu1–N1 = 2.072(4); Cu1–N2 = 2.063(4)	P2–Cu1–P1 = 101.56(4)	N2–Cu1–N1 = 79.75(14)	6.4(5)
[Cu(BIPHEP)(5,5'-Me$_2$bpy)]$^+$	Cu1–P16 = 2.2248(6); Cu1–P41 = 2.2515(6)	Cu1–N2 = 2.0321(18); Cu1–N15 = 2.0751(18)	P16–Cu1–P41 = 106.24(2)	N2–Cu1–N15 = 80.51(7)	−10.3(3)

(a) (b) (c) (d)
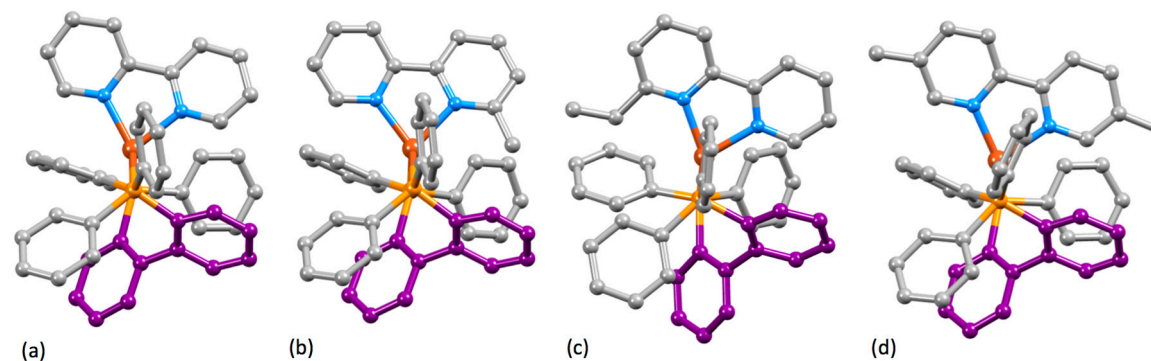
Figure 7. Comparisons of the distorted tetrahedral coordination spheres (viewed along the P...P vector) of copper(I) in (a) [Cu(BIPHEP)(bpy)]$^+$ (τ_4 = 0.81), (b) [Cu(BIPHEP)(6-Mebpy)]$^+$ (τ_4 = 0.85), (c) [Cu(BIPHEP)(6-Etbpy)]$^+$ (τ_4 = 0.78), and (d) [Cu(BIPHEP)(5,5'-Me$_2$bpy)]$^+$ (τ_4 = 0.80). The origin of the chirality is the twisted backbone of BIPHEP (shown in purple).

The copper atoms in the complexes exhibit distorted tetrahedral geometries, with τ_4 parameters [34] of 0.81 for [Cu(BIPHEP)(bpy)]$^+$, 0.85 for [Cu(BIPHEP)(6-Mebpy)]$^+$, 0.78 for [Cu(BIPHEP)(6-Etbpy)]$^+$, and 0.80 for [Cu(BIPHEP)(5,5′-Me$_2$bpy)]$^+$. For T_d symmetry, $\tau_4 = 1.00$, and the values observed here indicate a distortion towards a trigonal pyramidal geometry. Figure 7 displays the four [Cu(BIPHEP)(N^N)]$^+$ cations, each viewed along the P...P vector; the same enantiomer is shown for each complex. The Cu–P distances are typical (2.2248(6) to 2.2570(7) Å) and the same is true for the Cu–N distances (range = 2.0321(18) to 2.086(2) Å, Table 1). The P–Cu–P angles lie in the range 101.56(4)°–106.24(2)°. For the analogous POP and xantphos complexes with eight-membered rings, the bite angle of the coordinated phosphanes is around 113° for the complexes with 6-Mebpy or 6-Etbpy [18,19], and in the range 111.97(3)°–115.00(3)° for [Cu(POP)(bpy)][PF$_6$] and [Cu(xantphos)(bpy)][PF$_6$] [15–17]. As expected, the chelating 2,2′-bipyridine ligands exhibit similar N–Cu–N angles, in the range 79.75(14)°–80.65(10)°. The two rings of the bpy ligand are twisted in all the complex cations, with N–C–C–N torsion angles between 6.4(5)° in [Cu(BIPHEP)(6-Etbpy)]$^+$, and −12.1(4)° in [Cu(BIPHEP)(6-Mebpy)]$^+$.

There are no trends in the structural parameters as a function of the number or steric demands of the alkyl substituents attached to the bpy unit, and it appears that packing effects are dominant. In the complexes containing [Cu(BIPHEP)(bpy)][PF$_6$]$^+$, [Cu(BIPHEP)(6-Mebpy)]$^+$ and [Cu(BIPHEP)(5,5′-Me$_2$bpy)]$^+$, intracation π-stacking interactions occur between a phenyl ring of a PPh$_2$ group and one ring of the BIPHEP backbone (Figures 5 and 6b, and Figure S18 in the Supporting Information) although the angles between the ring planes of 25.7°, 15.1° and 18.0° mean that the interactions are not optimal. Short C–H...F cation...anion contacts feature in all of the structures, and the accommodation of solvent molecules in [Cu(BIPHEP)(bpy)][PF$_6$]·CH$_2$Cl$_2$, [Cu(BIPHEP)(6-Mebpy)][PF$_6$]·Et$_2$O·0.5H$_2$O and [Cu(BIPHEP)(5,5′-Me$_2$bpy)][PF$_6$]·CH$_2$Cl$_2$ also contributes to packing effects.

2.3. Electrochemical Behaviour

The electrochemical behaviour of the [Cu(BIPHEP)(N^N)][PF$_6$] compounds was investigated using cyclic voltammetry (CV), and cyclic voltammograms for CH$_2$Cl$_2$ solutions are shown in Figures S19–S22 (see Supporting Information). Each compound exhibits a reversible or quasi-reversible oxidation process (Table 2) assigned to a Cu$^+$/Cu^{2+} oxidation, but no ligand-based reduction processes were observed within the solvent-accessible window. For comparison, Table 2 also reports the oxidation potentials of [Cu(P^P)(bpy)][PF$_6$] and [Cu(P^P)(6-Mebpy)][PF$_6$] (P^P = POP and xantphos) [17,18], measured under the same conditions as the BIPHEP-containing compounds. For the BIPHEP complexes, the oxidation potentials increase on going from the complex with the unsubstituted bpy (+0.59 V), to 6-Mebpy (+0.72 V) and 6-Etbpy (+0.73 V). This follows the trend in the corresponding xantphos-containing compounds (Table 2), although, with the more flexible POP ligand, the introduction of the 6-methyl substituent has little effect. The trends for the BIPHEP-containing compounds are consistent with the introduction of the 6-alkyl substituent, hindering the flattening of the tetrahedral copper(I) towards square planar copper(II), thereby moving the oxidation to a higher potential. The Cu$^+$/Cu^{2+} oxidation occurs at similar potentials in [Cu(BIPHEP)(5,5′-Me$_2$bpy)][PF$_6$] and [Cu(BIPHEP)(bpy)][PF$_6$] (Table 2), indicating that the presence of methyl groups in these positions has little stabilizing effect on the copper(I) oxidation state. The data in Table 2 reveal that metal oxidation in [Cu(BIPHEP)(bpy)][PF$_6$] occurs at significantly lower potential than in [Cu(POP)(bpy)][PF$_6$] and [Cu(xantphos)(bpy)][PF$_6$], suggesting that the flattening of the copper coordination sphere that accompanies oxidation from Cu$^+$ to Cu^{2+} occurs more easily. This should also be reflected in the excited state lifetimes, which are discussed in the next section. We note that there is no clear correlation between the Cu$^+$/Cu^{2+} oxidation potential in solution and the τ_4 value (see Section 2.2), which gives a measure of the distortion away from a tetrahedral geometry (for which $\tau_4 = 1.00$) in the solid state.

Table 2. Cyclic voltammetric data for [Cu(BIPHEP)(N^N)][PF$_6$] complexes referenced to internal Fc/Fc$^+$ = 0.0 V; CH$_2$Cl$_2$ (dried) solutions, with [^{n}Bu$_4$N][PF$_6$] as the supporting electrolyte and a scan rate of 0.1 V s^{-1}. Processes are quasi-reversible.

Cation in [Cu(BIPHEP)(N^N)][PF$_6$]	$E_{1/2}^{ox}$/V	$E_{pc} - E_{pa}$/mV
[Cu(BIPHEP)(bpy)]$^+$	+0.59	100
[Cu(BIPHEP)(6-Mebpy)]$^+$	+0.72	129
[Cu(BIPHEP)(6-Etbpy)]$^+$	+0.73	133
[Cu(BIPHEP)(5,5'-Me$_2$bpy)]$^+$	+0.57	197
[Cu(POP)(bpy)]$^+$	+0.72 [a]	110 [a]
[Cu(POP)(6-Mebpy)]$^+$	+0.69 [b]	-
[Cu(xantphos)(bpy)]$^+$	+0.76 [a]	110 [a]
[Cu(xantphos)(6-Mebpy)]$^+$	+0.90 [a]	100 [a]

[a] Data taken from reference [17]. [b] Data taken from reference [18].

2.4. Photophysical Properties

The solution absorption spectra of the [Cu(BIPHEP)(N^N)][PF$_6$] compounds in CH$_2$Cl$_2$ are displayed in Figure 8 and absorption maxima are given in Table 3. The spectra for all four compounds are similar, with intense, high-energy (230–330 nm) absorptions arising from spin-allowed, ligand-based $\pi^* \leftarrow \pi$ transitions. The broad absorption, with λ_{max} close to 400 nm, is assigned to the MLCT band, and values of λ_{max} and ε_{max} vary little across the series of compounds.
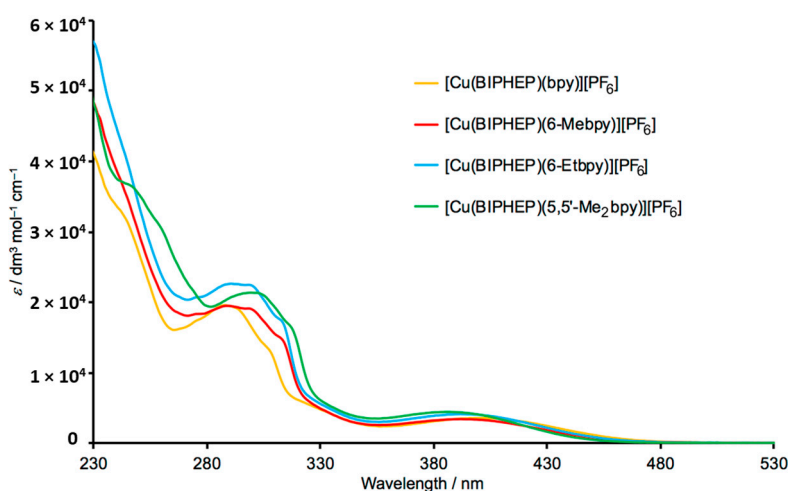
Figure 8. Solution absorption spectra of the [Cu(BIPHEP)(N^N)][PF$_6$] complexes (CH$_2$Cl$_2$, 3.5–5.3 × 10^{-5} mol dm^{-3}).

Table 3. Solution absorption maxima for the [Cu(BIPHEP)(N^N)][PF$_6$] complexes (CH$_2$Cl$_2$ with solution concentrations in the range 3.5–5.3 × 10^{-5} mol dm^{-3}).

| Cation in [Cu(BIPHEP)(N^N)][PF$_6$]	λ_{max}/nm (ε/dm^3 mol^{-1} cm^{-1}) Ligand-Based $\pi^* \leftarrow \pi$	MLCT
[Cu(BIPHEP)(bpy)]$^+$	244 sh (32,000), 291 (19,400), 309 sh (12,400)	407 (3500)
[Cu(BIPHEP)(6-Mebpy)]$^+$	292 (19,400), 301 (18,500), 316 sh (14,500)	400 (3400)
[Cu(BIPHEP)(6-Etbpy)]$^+$	292 (22,500), 301 (22,100), 315 sh (15,800)	400 (4000)
[Cu(BIPHEP)(5,5'-Me$_2$bpy)]$^+$	248 sh (36,200), 301 (21,300), 319 sh (15,200)	390 (4400)

When excited into the MLCT band at 390 nm, deaerated solutions of [Cu(BIPHEP)(bpy)][PF$_6$] did not show a detectable emission, while [Cu(BIPHEP)(6-Mebpy)][PF$_6$], [Cu(BIPHEP)(6-Etbpy)][PF$_6$] and [Cu(BIPHEP)(5,5'-Me$_2$bpy)][PF$_6$] exhibited weak emissions, with values of λ_{em}^{max} = 645, 636 and

641 nm, respectively (Figure S23 in Supporting Information). Since these emissions were so weak, we focused on solid-state and frozen-glass emission behaviour. Emission maxima, photoluminescence quantum yields (PLQY) and excited state lifetimes ($\tau_{1/2}$) are presented in Table 4. Powdered samples are yellow emitters with values of λ_{em}^{max}, in the range 558–583 nm (Figure 9a), and are similar to those observed for [Cu(PˆP)(bpy)][PF$_6$], [Cu(PˆP)(6-Mebpy)][PF$_6$] and [Cu(PˆP)(6-Etbpy)][PF$_6$], in which PˆP is POP or xantphos [17–19]. A blue shift in the emission maximum, upon going from liquid solution to a solid state, is consistent with previous observations of these families of compounds [19,22]. The highest PLQY for the solid-state compounds (Table 4) is 14% for [Cu(BIPHEP)(5,5'-Me$_2$bpy)][PF$_6$] and this also shows the longest excited state lifetime (8 μs). This may indicate better protection of the copper centre against quenchers (e.g., O$_2$ and H$_2$O) [22], although substitution in the 5,5'-positions, in the case of [Cu(POP)(5,5'-(CF$_3$)$_2$bpy)][PF$_6$] and [Cu(xantphos)(5,5'-(CF$_3$)$_2$bpy)][PF$_6$], proved less beneficial than a 6,6'-substitution pattern [17]. As noted earlier, we were not able to isolate [Cu(BIPHEP)(6,6'-Me$_2$bpy)][PF$_6$] and are not, therefore, able to compare the effects of going from 5,5'-Me$_2$bpy to 6,6'-Me$_2$bpy in the case of the BIPHEP co-ligand.

Table 4. Emission maxima, photoluminescence quantum yields (PLQY) and lifetimes ($\tau_{1/2}$) for [Cu(BIPHEP)(NˆN)][PF$_6$] complexes.

Cation in [Cu(BIPHEP)(NˆN)][PF$_6$]	Powder [a]			Frozen Glass (Me-THF, 77 K) [b]	
	λ_{em}^{max}/nm [c]	PLQY/%	$\tau_{1/2}$/μs	λ_{em}^{max}/nm [d]	$\tau_{1/2}$/μs
[Cu(BIPHEP)(bpy)]$^+$	566	4	3	615	7
[Cu(BIPHEP)(6-Mebpy)]$^+$	568	7	3	595	45
[Cu(BIPHEP)(6-Etbpy)]$^+$	583	3	1	590	53
[Cu(BIPHEP)(5,5'-Me$_2$bpy)]$^+$	558	14	8	600	49

[a] λ_{exc} = 365 nm; [b] λ_{exc} = 410 nm. [c] λ_{em}^{max} estimated error ± 2 nm. [d] λ_{em}^{max} estimated error ± 5 nm.
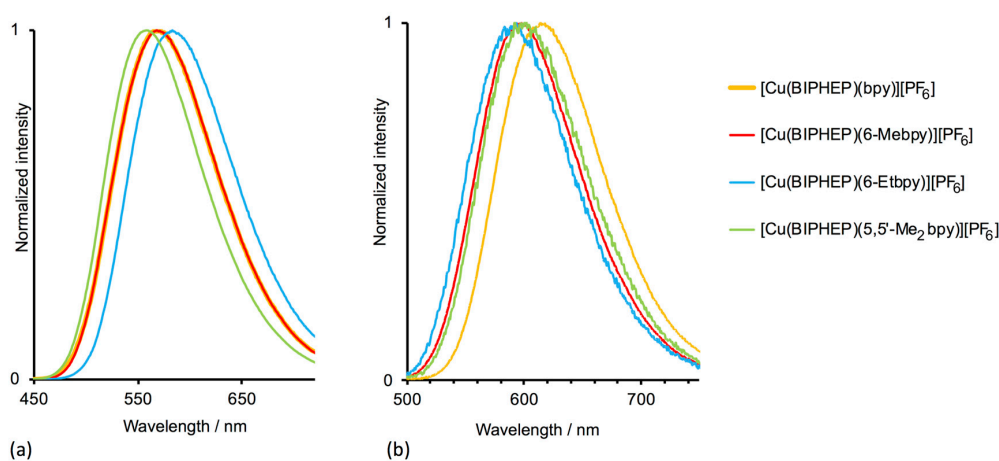
Figure 9. (**a**) Normalized emission spectra of the powdered [Cu(BIPHEP)(NˆN)][PF$_6$] compounds, λ_{exc} = 365 nm. The curves for [Cu(BIPHEP)(bpy)][PF$_6$] and [Cu(BIPHEP)(6-Mebpy)][PF$_6$] are virtually superimposed. (**b**) Normalized emission spectra of the [Cu(BIPHEP)(NˆN)][PF$_6$] complexes in frozen Me-THF at 77 K. λ_{exc} = 410 nm.

In order to investigate whether the [Cu(BIPHEP)(NˆN)][PF$_6$] compounds were TADF emitters, their emission and excited state lifetimes were recorded at low temperature and compared to their values at room temperature. Since the repopulation of the singlet excited state by reverse intersystem crossing is suppressed at low temperatures ($\Delta E > kT$), the excited state lifetime should be considerably longer, since phosphorescence from the triplet excited state should be the dominant process. The normalized emission spectra of the [Cu(BIPHEP)(NˆN)][PF$_6$] complexes in frozen Me-THF at 77 K are depicted in Figure 9b, and the emission maxima and excited state lifetimes are summarized in Table 4. A comparison

of the values of $\lambda_{em}{}^{max}$ in the powders at room temperature with those at 77 K reveals that the emission maxima are red-shifted for all the complexes, consistent with the triplet excited state being lower in energy than the singlet excited state. A significant extension of the excited state lifetimes is observed (Table 4), and, for the compounds in which the bpy bears alkyl substituents, values of $\tau_{1/2}$ are ca. 50 μs. These data are consistent with [Cu(BIPHEP)(N^N)][PF$_6$] (N^N = 6-Mebpy, 6-Etbpy and 5,5′-Me$_2$bpy) being TADF emitters. The increased excited state lifetime on going from 298 to 77 K is particularly noticeable for [Cu(BIPHEP)(6-Etbpy)][PF$_6$], where $\tau_{1/2}$ increases from 1 μs at room temperature to 53 μs at 77 K. At the same time, the temperature-induced red-shift in this complex is the smallest in the series, and at 77 K, it has an emission maximum at the shortest wavelength compared to others in the series. This raises the question as to whether other effects such as non-radiative decay processes occur in [Cu(BIPHEP)(6-Etbpy)][PF$_6$].

Since [Cu(BIPHEP)(5,5′-Me$_2$bpy)][PF$_6$] exhibited the highest PLQY and longest excited state lifetime in the solid state, we decided to conduct preliminary tests in LECs. Simple bilayer devices were fabricated by spin-coating a solution of [Cu(BIPHEP)(5,5′-Me$_2$bpy)][PF$_6$] on indium tin oxide-coated glass substrates, covered with a film of poly(3,4-ethylenedioxythiophene) polystyrene sulfonate. Devices were finished with the thermal evaporation of an aluminium cathode. LECs exhibited yellow electroluminescence with $\lambda_{em}{}^{max}$ = 586 nm, red-shifted with respect to the solid-state photoluminescence. However, even at a current density of 100 A m^{-2}, the maximum luminance was as low as 12 cd m^{-2}, with a maximum external quantum efficiency (EQE) of 0.03%. The LEC also showed only a short lifetime, with $t_{1/2}$ = 0.1 hours. In comparison, LECs containing [Cu(xantphos)(6-Mebpy)][PF$_6$], [Cu(xantphos)(6-Etbpy)][PF$_6$] and [Cu(POP)(6-Etbpy)][PF$_6$] in the emissive layers exhibit values of $t_{1/2}$ greater than 15, 40 and 80 h, respectively [18,19].

3. Materials and Methods

3.1. General

^{1}H and ^{13}C{^{1}H} and ^{31}P-NMR spectra were recorded on a Bruker Avance III-500 spectrometer (Bruker BioSpin AG, Fällanden, Switzerland) at 298 K. ^{1}H and ^{13}C-NMR chemical shifts were referenced, with respect to residual solvent peaks (δ TMS = 0), and ^{31}P-NMR chemical shifts, with respect to δ(85% aqueous H$_3$PO$_4$) = 0 ppm. Solution absorption and emission spectra were measured using a Shimadzu UV-2600 spectrophotometer and a Shimadzu RF-5301PC spectrofluorometer, respectively (Shimadzu Schweiz GmbH, 4153 Aesch, Switzerland). A Shimadzu LCMS-2020 instrument (Shimadzu Schweiz GmbH, 4153 Aesch, Switzerland) was used to record electrospray ionization (ESI) mass spectra; samples were introduced as MeCN solutions with added formic acid.

Quantum yields (CH$_2$Cl$_2$ solutions or powder samples) were measured with a Hamamatsu absolute photoluminescence quantum yield spectrometer C11347 Quantaurus-QY (Hamamatsu Photonics, 4500 Solothurn, Switzerland). Emission lifetimes and powder emission spectra were recorded using a Hamamatsu Compact Fluorescence lifetime Spectrometer C11367 Quantaurus-Tau (Hamamatsu Photonics), with an LED light source with λ_{exc} = 365 nm. Low temperature emission and lifetime measurements were made using an Edinburgh Instruments LP920-KS instrument (Edinburgh Instruments, Livingston, UK), in frozen 2-methyloxolane (Me-THF); a 410 nm excitation was obtained from pulsed third-harmonic radiation from a Quantel Brilliant b Nd:YAG laser (Quantal Laser, Lumibird, 22300 Lannion, France), equipped with a Rainbow optical parameter oscillator. The laser pulse duration and pulse frequency were ~10 ns and 10 Hz, respectively, with a typical pulse energy of 7 mJ. An iCCD camera (Andor, Oxford Instruments GmbH, Wiesbaden, Germany) was used for detection of the spectra. Single-wavelength kinetics were recorded using a photomultiplier tube.

6-Methyl-2,2′-bipyridine (6-Mebpy) and 6-ethyl-2,2′-bipyridine (6-Etbpy) [35] and [Cu(MeCN)$_4$][PF$_6$] [36] were prepared following the literature procedures. BIPHEP was bought from Alfa Aesar (Alfa Aesar GmbH, 76185 Karlsruhe, Germany), and 2,2′-bipyridine (bpy), 5,5′-dimethyl-2,2′-bipyridine

(5,5′-Me$_2$bpy) and 6,6′-dimethyl-2,2′-bipyridine (6,6′-Me$_2$bpy) from Sigma-Aldrich (Merck, 9470 Buchs, Switzerland). All chemicals were used as received.

3.2. [Cu(BIPHEP)(bpy)][PF$_6$]

A colourless solution of bpy (39 mg, 0.25 mmol) and BIPHEP (131 mg, 0.25 mmol) in CH$_2$Cl$_2$ (20 mL) was added to a colourless solution of [Cu(MeCN)$_4$][PF$_6$] (93 mg, 0.25 mmol) in CH$_2$Cl$_2$ (20 mL), turning the solution yellow. After stirring at room temperature for 2 h, the solvent was removed in vacuo. The crude product was redissolved in CH$_2$Cl$_2$ and [Cu(BIPHEP)(bpy)][PF$_6$] (63 mg, 0.071 mmol, 28%), precipitated as a yellow powder by layering with Et$_2$O. ^{1}H-NMR (500 MHz, acetone-d_6, 298 K): δ/ppm 8.76 (dt, *J* = 8.2, 1.0 Hz, 2H, H^{A3}), 8.42 (dd, *J* = 5.2, 1.4 Hz, 2H, H^{A6}), 8.29 (td, *J* = 7.9, 1.6 Hz, 2H, H^{A4}), 7.67 (m, 2H, H^{A5}), 7.42–7.37 (m, 2H, H$^{D4/D4'}$), 7.34–7.26 (overlapping m, 16H, H$^{D2+D2'+D3/D3'+D4/D4'+C5}$), 7.26–7.17 (overlapping m, 6H, H$^{D3/D3'+C4}$), 7.10 (m, 2H, H^{C6}), 6.81 (m, 2H, H^{C3}). ^{13}C{^{1}H} NMR (126 MHz, acetone-d_6, 298 K): δ/ppm 152.9 (t, J_{PC} = 2 Hz, C^{A2}), 151.4 (C^{A6}), 146.5 (t, J_{PC} = 9 Hz, C^{C1}), 140.2 (C^{A4}), 135.7 (t, J_{PC} = 3.5 Hz, C^{C6}), 135.0 (t, J_{PC} = 8 Hz, C$^{D2/D2'}$), 134.5 (t, J_{PC} = 8 Hz, C$^{D2/D2'}$), 132.9 (t, J_{PC} = 18 Hz, C$^{D1/D1'}$), 132.2 (t, J_{PC} = 14 Hz, C^{C2}), 131.6 (t, J_{PC} = 18 Hz, C$^{D1/D1'}$), 131.6 (C^{C3}), 131.5 (t, J_{PC} = 1 Hz, C$^{D4/D4'}$), 131.2 (t, J_{PC} = 1 Hz, C$^{D4/D4'}$), 130.6 (C^{C5}), 130.0 (t, J_{PC} = 5 Hz, C$^{D3/D3'}$), 129.4 (t, J_{PC} = 5 Hz, C$^{D3/D3'}$), 128.6 (t, J_{PC} = 3 Hz, C^{C4}), 127.2 (C^{A5}), 123.8 (C^{A3}). ^{31}P{^{1}H} NMR (202 MHz, acetone-d_6, 298 K): δ/ppm −1.2 (broad, FWHM = 270 Hz, BIPHEP), −142.5 (septet, J_{PF} = 700 Hz, [PF$_6$]$^-$). ESI MS: *m/z* 741.10 [M–PF$_6$]$^+$ (base peak, calc. 741.16). Found C 61.53, H 4.37, N 3.22; C$_{46}$H$_{36}$CuF$_6$N$_2$P$_3$·H$_2$O requires C 61.03, H 4.23, N 3.09.

3.3. [Cu(BIPHEP)(6-Mebpy)][PF$_6$]

A colourless solution of 6-Mebpy (43 mg, 0.25 mmol) and BIPHEP (131 mg, 0.25 mmol) in CH$_2$Cl$_2$ (20 mL) was added to a colourless solution of [Cu(MeCN)$_4$][PF$_6$] (93 mg, 0.25 mmol) in CH$_2$Cl$_2$ (20 mL), turning the solution yellow. After stirring at room temperature for 2 h, the solvent was removed under reduced pressure. The crude product was redissolved in CH$_2$Cl$_2$ and layered with Et$_2$O, to precipitate [Cu(BIPHEP)(6-Mebpy)][PF$_6$] (202 mg, 0.23 mmol, 92%) as a yellow powder. ^{1}H-NMR (500 MHz, acetone-d_6, 298 K): δ/ppm 8.72 (dt, *J* = 8.3, 1.0 Hz, 1H, H^{A3}), 8.62 (d, *J* = 7.9 Hz, 1H, H^{B3}), 8.29–8.21 (overlapping m, 2H, H^{B4+A4}), 8.04 (dt, *J* = 5.2, 0.8 Hz, 1H, H^{A6}), 7.73 (dd, *J* = 7.8, 0.9 Hz, 1H, H^{B5}), 7.54 (m, 1H, H^{A5}), 7.46–7.10 (overlapping m, 26H, H$^{D2+D2'+D3+D3'+D4+D4'+C4+C4'+C5+C5'+C6+C6'}$), 6.99 (m, 1H, H$^{C3/C3'}$), 6.88 (m, 1H, H$^{C3/C3'}$), 2.58 (s, 3H, H^{Me}). ^{13}C{^{1}H} NMR (126 MHz, acetone-d_6, 298 K): δ/ppm 160.5 (C^{B6}), 153.5 (C$^{A2/B2}$), 152.7 (C$^{A2/B2}$), 151.0 (C^{A6}), 145.7 (br, C$^{C1+C1'}$), 140.6 (C$^{A4/B4}$), 140.2 (C$^{A4/B4}$), 136.2 (br, C$^{C6/C6'}$), 135.2 (br, overlapping, C$^{D2/D2'}$), 134.2 (C$^{D2/D2'}$), 134.1 (C$^{D2/D2'}$), 129.45 (C$^{D3/D3'}$), 129.4 (C$^{D3/D3'}$), 128.8 (br, C$^{C4+C4'}$), 127.6 (C^{B5}), 127.0 (C^{A5}), 123.9 (C^{A3}), 121.4 (C^{B3}); signals for C^{C3}, C^{C5}, C^{C1}, C^{C2}, C^{D1} were poorly resolved. ^{31}P{^{1}H} NMR (202 MHz, acetone-d_6, 298 K): δ/ppm −1.3 (broad, FWHM = 428 Hz, BIPHEP) −3.7 (broad, FWHM = 401 Hz, BIPHEP), −144.2 (septet, J_{PF} = 700 Hz, [PF$_6$]$^-$). ESI MS: *m/z* 755.16 [M–PF$_6$]$^+$ (base peak, calc. 755.18). Found C 61.89, H 4.83, N 3.38; C$_{47}$H$_{38}$CuF$_6$N$_2$P$_3$·H$_2$O requires C 61.41, H 4.39, N 3.05.

3.4. [Cu(BIPHEP)(6-Etbpy)][PF$_6$]

A solution of 6-Etbpy (46 mg, 0.25 mmol) and BIPHEP (131 mg, 0.25 mmol) in CH$_2$Cl$_2$ (20 mL) was added to a solution of [Cu(MeCN)$_4$][PF$_6$] (93 mg, 0.25 mmol) in CH$_2$Cl$_2$ (20 mL), causing an immediate change from colourless to yellow. After stirring at room temperature for 2 h, the solvent was removed in vacuo. The crude material was redissolved in CH$_2$Cl$_2$. Layering with Et$_2$O precipitated [Cu(BIPHEP)(6-Etbpy)][PF$_6$] (208 mg, 0.23 mmol, 92%) as a yellow powder. ^{1}H-NMR (500 MHz, acetone-d_6, 298 K): δ/ppm 8.72 (d, *J* = 8.2 Hz, 1H, H^{A3}), 8.62 (d, *J* = 7.8 Hz, 1H, H^{B3}), 8.31 (t, *J* = 7.9 Hz, 1H, H^{B4}), 8.24 (td, *J* = 7.6, 1.6 Hz, 1H, H^{A4}), 7.91 (m, 1H, H^{A6}), 7.79 (d, *J* = 7.7 Hz, 1H, H^{B5}), 7.51 (m, 1H, H^{A5}), 7.42–7.12 (overlapping m, 25H, H$^{D4+D4'+C5+C5'+D2+D2'+D3+D3'+C4+C4'+C6/C6'}$), 7.08 (m, 1H, C$^{C6/C6'}$), 7.00 (m, 1H, H^{C3}), 6.88 (m, 1H, H^{C3}), 3.03 (q, *J* = 7.8 Hz, 2H, H^{Et}), 1.08 (t, *J* = 7.6 Hz, 3H, H^{Et}). ^{13}C{^{1}H} (126 MHz, acetone-d_6, 298 K): 164.8 (C^{B6}), 153.6 (C$^{A2/B2}$), 152.4 (C$^{A2/B2}$), 151.0 (C^{A6}), 145.8 (C$^{C1/C1'}$),

145.6 ($C^{C1/C1'}$), 140.8 (C^{B4}), 140.2 (C^{A4}), 136.1 ($C^{C6+C6'}$), 135.3 (overlapping m, $C^{D2/D2'}$), 134.2 ($C^{D2/D2'}$), 134.0 ($C^{D2/D2'}$), 132.7–131.6 (overlapping m, $C^{D1+D1'+C2+C2'}$), 131.5 (br, $C^{C3+C3'}$), 131.0 ($C^{D4/D4'}$), 130.9 ($C^{D4/D4'}$), 130.8 ($C^{D4/D4'}$), 130.5 ($C^{D4/D4'}$), 130.0 and 129.8 (br, overlapping m, $C^{D3/D3'+C5+C5'}$), 129.4 (br, overlapping m, $C^{D3/D3'}$), 128.7 (br, $C^{C4/C4'}$), 128.5 (br, $C^{C4/C4'}$), 126.9 (C^{A5}), 125.4 (C^{B5}), 123.9 (C^{A3}), 121.6 (C^{B3}), 35.5 (C^{Et}), 13.2 (C^{Et}); see text discussion. $^{31}P\{^1H\}$ NMR (162 MHz, acetone-d_6, 300 K) δ/ppm −1.3 (broad, FWHM = 320 Hz, BIPHEP), −4.0 (broad, FWHM = 320 Hz, BIPHEP), −144.2 (septet, J_{PF} = 708 Hz, [PF_6]$^−$); see text discussion. ESI MS: *m/z* 769.28 [M–PF_6]$^+$ (base peak, calc. 769.20). Found C 62.40, H 4.98, N 3.22; $C_{48}H_{40}CuF_6N_2P_3 \cdot 0.5H_2O$ requires C 62.37, H 4.47, N 3.03.

3.5. [Cu(BIPHEP)(5,5′-Me₂bpy)][PF₆]

A solution of 5,5′-Me$_2$bpy (46 mg, 0.25 mmol) and BIPHEP (131 mg, 0.25 mmol) in CH_2Cl_2 (20 mL) was added to a solution of [Cu(MeCN)$_4$][PF_6] (93 mg, 0.25 mmol) in CH_2Cl_2 (20 mL). The yellow reaction mixture was stirred at room temperature for 2 h, and then solvent was removed under reduced pressure. The crude product was redissolved in CH_2Cl_2 and layering with Et$_2$O led to the precipitation of yellow [Cu(BIPHEP)(5,5′-Me$_2$bpy)][PF_6] (215 mg, 0.23 mmol, 92%). ^{1}H-NMR (500 MHz, acetone-d_6, 298 K): δ/ppm ^{1}H-NMR (500 MHz, acetone-d_6, 298 K) δ /ppm 8.55 (d, *J* = 8.2 Hz, 2H, H^{B3}), 8.04 (m, 2H, H^{B4}), 7.96 (m, 2H, H^{B6}), 7.44–7.39 (m, 2H, H$^{D4/D4'}$), 7.38–7.29 (overlapping m, 12H, H$^{D2/D2'+D3/D3'+D4/D4'+C5}$), 7.27–7.19 (m, 10H, H$^{D2/D2'+D3/D3'+C4}$), 7.15 (m, 2H, H^{C6}), 6.76 (m, 2H, H^{C3}), 2.30 (s, 6H, H^{Me}). $^{13}C\{^1H\}$ NMR (126 MHz, acetone-d_6, 298 K) δ /ppm 151.5 (C^{B6}), 150.5 (t, *J* = 2 Hz, C^{B2}), 145.7 (t, *J* = 10 Hz, C^{C1}), 140.2 (C^{B4}), 137.3 (C^{B5}), 135.8 (t, *J* = 4 Hz, C^{C6}), 135.2 (t, *J* = 9 Hz, $C^{D2/D2'}$), 134.6 (t, *J* = 8 Hz, $C^{D2/D2'}$), 132.8 (t, *J* = 18 Hz, $C^{D1/D1'}$), 132.2 (t, *J* = 14 Hz, C^{C2}), 131.7 (t, *J* = 3 Hz, C^{C3}), 131.6 ($C^{D4/D4'}$), 131.3 (t, *J* = 18 Hz, $C^{D1/D1'}$), 131.1 ($C^{D4/D4'}$), 130.6 (C^{C5}), 130.0 (t, *J* = 5 Hz, $C^{D3/D3'}$), 129.3 (t, *J* = 5 Hz, $C^{D3/D3'}$), 128.6 (t, *J* = 3 Hz, C^{C4}), 122.8 (C^{B3}), 18.1 (C^{Me}). $^{31}P\{^1H\}$ NMR (162 MHz, acetone-d_6, 300 K) δ/ppm −0.6 (broad, FWHM = 350 Hz, BIPHEP), −144.2 (septet, J_{PF} = 708 Hz, [PF_6]$^−$). ESI MS: *m/z* 769.28 [M–PF_6]$^+$ (base peak, calc. 769.20). Found C 58.24, H 4.30, N 3.02; $C_{48}H_{40}CuF_6N_2P_3 \cdot CH_2Cl_2$ requires C 58.84, H 4.23, N 2.80.

3.6. Crystallography

Single crystal X-ray diffraction data were collected on a Bruker Kappa Apex2 diffractometer with data reduction, solution and refinement, using the programs APEX [37] and CRYSTALS [38]. Structural analysis used the program Mercury v. 4.1.2 [39,40].

3.7. [Cu(BIPHEP)(bpy)][PF₆]·CH₂Cl₂

$C_{47}H_{38}Cl_2CuF_6N_2P_3$, *M* = 972.19, yellow plate, monoclinic, space group $P2_1/c$, *a* = 14.3304(6), *b* = 15.4136(6), *c* = 20.6025(7) Å, β = 105.844(2)°, *U* = 4377.8(3) Å^3, *Z* = 4, D_c = 1.475 Mg m$^{−3}$, μ(Cu-Kα) = 3.397 mm$^{−1}$, *T* = 123 K. Total 46,656 reflections, 8189 unique, R_{int} = 0.071. Refinement of 6109 reflections (550 parameters) with *I* >2σ(*I*) converged at final R_1 = 0.0505 (R_1 all data = 0.0733), wR_2 = 0.1151 (wR_2 all data = 0.1308), gof = 0.9710. CCDC 1958102.

3.8. [Cu(BIPHEP)(6-Mebpy)][PF₆]·Et₂O·0.5H₂O

$C_{51}H_{49}CuF_6N_2O_{1.5}P_3$, *M* = 984.42, yellow block, monoclinic, space group $C2/c$, *a* = 29.5271(19), *b* = 16.7361(11), *c* = 20.5516(14) Å, β = 111.249(2)°, *U* = 9465.5(11) Å^3, *Z* = 8, D_c = 1.381 Mg m$^{−3}$, μ(Cu-Kα) = 2.157 mm$^{−1}$, *T* = 123 K. Total 31,108 reflections, 8537 unique, R_{int} = 0.023. Refinement of 8430 reflections (584 parameters) with *I* >2σ(*I*) converged at final R_1 = 0.0540 (R_1 all data = 0.0544), wR_2 = 0.1197 (wR_2 all data = 0.1197), gof = 1.0146. CCDC 1958100.

3.9. [Cu(BIPHEP)(6-Etbpy)][PF₆]

$C_{48}H_{40}CuF_6N_2P_3$, *M* = 915.31, yellow block, triclinic, space group $P−1$, *a* = 10.5819(11), *b* = 13.4147(14), *c* = 15.0134(16) Å, α = 93.766(3) β = 100.826(3), γ = 92.405(3)°, *U* = 2085.5(4) Å^3,

$Z = 2$, $D_c = 1.457$ Mg m^{-3}, μ(Cu-Kα) = 2.377 mm^{-1}, $T = 123$ K. Total 29,365 reflections, 7594 unique, $R_{int} = 0.032$. Refinement of 6965 reflections (541 parameters) with $I > 2\sigma(I)$ converged at final $R_1 = 0.0412$ (R_1 all data = 0.0502), $wR_2 = 0.0822$ (wR_2 all data = 0.1385), gof = 1.3893. CCDC 1958101.

3.10. [Cu(BIPHEP)(5,5′-Me₂bpy)][PF₆]·CH₂Cl₂

C$_{49}$H$_{42}$Cl$_2$CuF$_6$N$_2$P$_3$, $M = 1000.25$, yellow block, triclinic, space group $P{-}1$, $a = 10.9543(6)$, $b = 10.9953(6)$, $c = 18.8408(11)$ Å, $\alpha = 94.9723(17)$, $\beta = 92.9633(18)$, $\gamma = 96.7453(17)°$, $U = 2240.7(2)$ Å^3, $Z = 2$, $D_c = 1.482$ Mg m^{-3}, μ(Cu-Kα) = 3.334 mm^{-1}, $T = 123$ K. Total 29,278 reflections, 7850 unique, $R_{int} = 0.030$. Refinement of 7808 reflections (568 parameters) with $I > 2\sigma(I)$ converged at final $R_1 = 0.0453$ (R_1 all data = 0.0453), $wR_2 = 0.0461$ (wR_2 all data = 0.0461), gof = 1.1280. CCDC 1958099.

4. Conclusions

We have prepared and characterized the compounds [Cu(BIPHEP)(bpy)][PF₆], [Cu(BIPHEP)(6-Mebpy)][PF₆], [Cu(BIPHEP)(6-Etbpy)][PF₆] and [Cu(BIPHEP)(5,5′-Me₂bpy)][PF₆]. ^{1}H, ^{13}C{^{1}H} and ^{31}P{^{1}H} NMR spectra, including the use of 2D methods, reveal dynamic processes involving the BIPHEP ligand. The single crystal structures of [Cu(BIPHEP)(bpy)][PF₆]·CH₂Cl₂, [Cu(BIPHEP)(5,5′-Me₂bpy)][PF₆]·CH₂Cl₂, [Cu(BIPHEP)(6-Mebpy)][PF₆]·Et₂O·0.5H₂O and [Cu(BIPHEP)(6-Etbpy)][PF₆] were determined and confirmed distorted tetrahedral {Cu(PˆP)(NˆN)} coordination environments. Each compound shows a quasi-reversible Cu$^+$/Cu^{2+} process, which moves to a higher potential upon the introduction of 6-methyl or 6-ethyl substituent into the bpy unit. The [Cu(BIPHEP)(NˆN)][PF₆] compounds are weak emitters in the deaerated solution, whereas powdered samples are yellow emitters at room temperature, with values of λ_{em}^{max} between 558 and 583 nm, and PLQY values up to 14%. Evidence that the compounds with NˆN = 6-Mebpy, 6-Etbpy and 5,5′-Me₂bpy exhibit TADF comes from the fact that their excited state lifetimes increase from $\tau_{1/2} < 8$ μs to $\tau_{1/2}$ values of up to 53 μs on cooling from room temperature to 77 K, and that the emission maxima are red-shifted.

References

1. Bizzarri, C.; Spuling, E.; Knoll, D.M.; Volz, D.; Bräse, S. Sustainable metal complexes for organic light-emitting diodes (OLEDs). *Coord. Chem. Rev.* **2018**, *373*, 49–82. [CrossRef]

2. Volz, D.; Wallesch, M.; Fléchon, C.; Danz, M.; Verma, A.; Navarro, J.M.; Zink, D.M.; Bräse, S.; Baumann, T. From iridium and platinum to copper and carbon: new avenues for more sustainability in organic light-emitting diodes. *Green Chem.* **2015**, *17*, 1988–2011. [CrossRef]

3. Fresta, E.; Costa, R.D. Beyond traditional light-emitting electrochemical cells—A review of new device designs and emitters. *J. Mater. Chem. C* **2017**, *5*, 5643–5675. [CrossRef]

4. Elie, M.; Gaillard, S.; Renaud, J.L. *Light-Emitting Electrochemical Cells: Concepts, Advances and Challenges*; Costa, R.D., Ed.; Springer International Publishing: New York, NY, USA, 2017. [CrossRef]

5. Salehi, A.; Fu, X.; Shin, D.-H.; So, F. Recent Advances in OLED Optical Design. *Adv. Funct. Mater.* **2019**, *29*, 1808803. [CrossRef]

6. Luo, D.; Chen, Q.; Liu, B.; Qiu, Y. Emergence of Flexible White Organic Light-Emitting Diodes. *Polymers* **2019**, *11*, 384. [CrossRef]

7. Wong, M.Y.; Zysman-Colman, E. Purely Organic Thermally Activated Delayed Fluorescence Materials for Organic Light-Emitting Diodes. *Adv. Mater.* **2017**, *29*, 1605444. [CrossRef]

8. Yerson, H. (Ed.) *Highly Eficient OLEDs: Materials Based on Thermally Activated Delayed Fluorescence*; John Wiley & Sons: Weinheim, Germany, 2019; ISBN 978-3-527-33900-6.

9. Czerwieniec, R.; Leitl, M.J.; Homeier, H.H.H.; Yerson, H. Cu(I) complexes—Thermally activated delayed fluorescence. Photophysical approach and material design. *Coord. Chem. Rev.* **2016**, *325*, 2–28. [CrossRef]

10. Bergmann, L.; Zink, D.M.; Bauman, T.; Volz, D.; Bräse, S. Metal-Oragnic and Organic TADF Materials: Status, Challenges and Characterization. *Top. Curr. Chem.* **2016**, *374*, 22. [CrossRef]

11. Yang, Z.; Mao, Z.; Xie, Z.; Zhang, Y.; Liu, S.; Zhao, J.; Xu, J.; Chi, Z.; Aldred, M.P. Recent Advances in Organic Thermally Activated Delayed Fluorescence Materials. *Chem. Soc. Rev.* **2017**, *46*, 915–1016. [CrossRef]

12. Buckner, M.T.; McMillin, D.R. Photoluminescence from copper(I) complexes with low-lying metal-to-ligand charge transfer excited states. *J. Chem. Soc. Chem. Commun.* **1978**, 759–761. [CrossRef]

13. Rader, R.A.; McMillin, D.R.; Buckner, M.T.; Matthews, T.G.; Casadonte, D.J.; Lengel, R.K.; Whittaker, S.B.; Darmon, L.M.; Lytle, F.E. Photostudies of 2,2′-bipyridine bis(triphenylphosphine)copper(1+), 1,10-phenanthroline bis(triphenylphosphine)copper(1+), and 2,9-dimethyl-1,10-phenanthroline bis(triphenylphosphine) copper(1+) in solution and in rigid, low-temperature glasses. Simultaneous multiple emissions from intraligand and charge-transfer states. *J. Am. Chem. Soc.* **1981**, *103*, 5906–5912. [CrossRef]

14. Kramer, P.C.J.; Van Leeuwen, P.W.N.M.; Reek, J.N.H. Wide Bite Angle Diphosphines: Xantphos Ligands in Transition Metal Complexes and Catalysis. *Acc. Chem. Rev.* **2001**, *34*, 895–904. [CrossRef]

15. Costa, R.D.; Tordera, D.; Ortí, E.; Bolink, H.J.; Schönle, J.; Graber, S.; Housecroft, C.E.; Constable, E.C.; Zampese, J.A. Copper(I) complexes for sustainable light-emitting electrochemical cells. *J. Mater. Chem. C* **2011**, *21*, 16108–16118. [CrossRef]

16. Yang, L.; Feng, J.-K.; Ren, A.-M.; Zhang, M.; Ma, Y.-G.; Liu, X.-D. Structures, Electronic States and Electroluminescent Properties of a Series of Cu^I Complexes. *Eur. J. Inorg. Chem.* **2005**, *2005*, 1867–1879. [CrossRef]

17. Keller, S.; Brunner, F.; Junquera-Hernández, J.M.; Pertegás, A.; La-Placa, M.-G.; Prescimone, A.; Constable, E.C.; Bolink, H.J.; Ortí, E.; Housecroft, C.E. CF$_3$ Substitution of [Cu(PˆP)(bpy)][PF$_6$] complexes: Effects on Photophysical Properties and Light-emitting Electrochemical Cell Performance. *ChemPlusChem* **2018**, *83*, 217–229. [CrossRef]

18. Keller, S.; Constable, E.C.; Housecroft, C.E.; Neuburger, M.; Prescimone, A.; Longo, G.; Pertegás, A.; Sessolo, M.; Bolink, H.J. [Cu(bpy)(PˆP)]$^+$ containing light-emitting electrochemical cells: improving performance through simple substitution. *Dalton Trans.* **2014**, *43*, 16593–16596. [CrossRef]

19. Keller, S.; Pertegás, A.; Longo, G.; Martínez, L.; Cerdá, J.; Junquera-Hernández, J.M.; Prescimone, A.; Constable, E.C.; Housecroft, C.E.; Ortí, E.; et al. Shine bright or live long: substituent effects in [Cu(NˆN)(PˆP)]$^+$-based light-emitting electrochemical cells where NˆN is a 6-substituted 2,2′-bipyridine. *J. Mater. Chem. C* **2016**, *4*, 3857–3871. [CrossRef]

20. Fresta, E.; Volpi, G.; Milanesio, M.; Garino, C.; Barolo, C.; Costa, R.D. Novel Ligand and Device Designs for Stable Light-Emitting Electrochemical Cells Based on Heteroleptic Copper(I) Complexes. *Inorg. Chem.* **2018**, *57*, 10469–10479. [CrossRef]

21. Brunner, F.; Martínez-Sarti, L.; Keller, S.; Pertegás, A.; Prescimone, A.; Constable, E.C.; Bolink, H.J.; Housecroft, C.E. Peripheral halo-functionalization in [Cu(NˆN)(PˆP)]$^+$ emitters: influence on the performances of light-emitting electrochemical cells. *Dalton Trans.* **2016**, *45*, 15180–15192. [CrossRef]

22. Alkan-Zambada, M.; Keller, S.; Martínez-Sarti, L.; Prescimone, A.; Junquera-Hernández, J.M.; Constable, E.C.; Bolink, H.J.; Sessolo, M.; Ortí, E.; Housecroft, C.E. [Cu(PˆP)(NˆN)][PF$_6$] compounds with bis(phosphane) and 6-alkoxy, 6-alkylthio, 6-phenyloxy and 6-phenylthio-substituted 2,2′-bipyridine ligands for light-emitting electrochemical cells. *J. Mater. Chem. C* **2018**, *6*, 8460–8471. [CrossRef]

23. Keller, S.; Prescimone, A.; Bolink, H.J.; Sessolo, M.; Longo, G.; Martínez-Sarti, L.; Junquera-Hernández, J.-M.; Constable, E.C.; Ortí, E.; Housecroft, C.E. Luminescent copper(I) complexes with bisphosphane and halogen-substituted 2,2′-bipyridine ligands. *Dalton Trans.* **2018**, *47*, 14263–14276. [CrossRef] [PubMed]

24. Brunner, F.; Babaei, A.; Pertegás, A.; Junquera-Hernández, J.M.; Prescimone, A.; Constable, E.C.; Bolink, H.J.; Sessolo, M.; Ortí, E.; Housecroft, C.E. Phosphane tuning in heteroleptic [Cu(NˆN)(PˆP)]$^+$ complexes for light-emitting electrochemical cells. *Dalton Trans.* **2019**, *48*, 446–460. [CrossRef] [PubMed]

25. Keller, S.; Prescimone, A.; Constable, E.C.; Housecroft, C.E. Copper(I) and silver(I) complexes of 9,9-dimethyl-4,5-bis(di-tert-butylphosphino)xanthene: photophysical properties and structural rigidity under pressure. *Photochem. Photobiol Sci.* **2018**, *17*, 375–385. [CrossRef] [PubMed]

26. Groom, C.R.; Bruno, I.J.; Lightfoot, M.P.; Ward, S.C. The Cambridge Structural Database. *Acta Cryst.* **2016**, *B72*, 171–179. [CrossRef]

27. Shi, Y.; Liu, X.; Shan, Y.; Zhang, X.; Kong, W.; Lu, Y.; Tan, Z.; Li, X.-L. Naked-eye repeatable off–on–off and on–off–on switching luminescence of copper(I)-1*H*-imidazo[4,5-*f*][1,10]phenanthroline complexes with reversible acid–base responses. *Dalton Trans.* **2019**, *48*, 2430–2441. [CrossRef]

28. Saito, K.; Tsukuda, T.; Tsubomura, T. Synthesis and Luminescence of New Cu(I) Complexes Containing a Binap Ligand and a Diimine Ligand. *Bull. Chem. Soc. Jpn.* **2006**, *79*, 437–441. [CrossRef]

29. Feng, X.-Y.; Xin, X.-L.; Guo, Y.-M.; Chen, L.-L.; Liang, Y.-Y.; Xu, M.; Li, X.-L. Synthesis, structure and solid luminescence of copper(I)–bromodiimine–diphosphine complexes. *Polyhedron* **2015**, *101*, 23–28. [CrossRef]

30. Tan, C.-H.; Ma, X.; Zhu, Q.-L.; Huang, Y.-H.; Fu, R.-B.; Hu, S.-M.; Sheng, T.-L.; Wu, X.-T. Syntheses, crystal structures and properties of dinuclear copper(I) complexes. *J. Mol. Struct.* **2012**, *1007*, 26–30. [CrossRef]

31. Oczipka, P.; Müller, D.; Leitner, W.; Franciò, G. Enantiodivergent asymmetric catalysis with the *tropos* BIPHEP ligand and a proline derivative as chiral selector. *Chem. Sci.* **2016**, *7*, 678–683. [CrossRef]

32. *Spartan '16, v. 2.0.9*, Wavefunction Inc.: Irvine, CA, USA, 2017.

33. Brunner, F.; Graber, S.; Baumgartner, Y.; Häussinger, D.; Prescimone, A.; Constable, E.C.; Housecroft, C.E. The effects of introducing sterically demanding aryl substituents in [Cu(NˆN)(PˆP)]$^+$ complexes. *Dalton Trans.* **2017**, *46*, 6379–6391. [CrossRef]

34. Yang, L.; Powell, D.R.; Houser, R.P. Structural variation in copper(I) complexes with pyridylmethylamide ligands: structural analysis with a new four-coordinate geometry index, τ_4. *Dalton Trans.* **2007**, 955–964. [CrossRef] [PubMed]

35. Shaul, M.; Cohen, Y. Novel Phenanthroline-Containing Trinuclear Double-Stranded Helicates: Self-Recognition between Helicates with Phenanthroline and Bipyridine Binding Sites. *J. Org. Chem.* **1999**, *64*, 9358–9364. [CrossRef]

36. Kubas, G.J. Tetrakis(Acetonitrile)Copper(I) Hexafluorophosphate. *Inorg. Synth.* **1979**, *19*, 90–92. [CrossRef]

37. *APEX2, version 2 User Manual, M86-E01078*, Bruker Analytical X-ray Systems Inc.: Madison, WI, USA, 2006.

38. Betteridge, P.W.; Carruthers, J.R.; Cooper, R.I.; Prout, K.; Watkin, D.J. CRYSTALS version 12: Software for guided crystal structure analysis. *J. Appl. Cryst.* **2003**, *36*, 1487. [CrossRef]

39. Macrae, C.F.; Edgington, P.R.; McCabe, P.; Pidcock, E.; Shields, G.P.; Taylor, R.; Towler, M.; van de Streek, J. Mercury: visualization and analysis of crystal structures. *J. Appl. Cryst.* **2006**, *39*, 453–457. [CrossRef]

40. Macrae, C.F.; Bruno, I.J.; Chisholm, J.A.; Edgington, P.R.; McCabe, P.; Pidcock, E.; Rodriguez-Monge, L.; Taylor, R.; van de Streek, J.; Wood, P.A. Mercury CSD 2.0 - new features for the visualization and investigation of crystal structures. *J. Appl. Cryst.* **2008**, *41*, 466–470. [CrossRef]

Sample Availability: Limited samples of the NˆN ligands are available from the authors.